

Optical chirality without optical activity: How surface plasmons give a twist to light

Aurélien Drezet, Cyriaque Genet, Jean-Yves Laluet and Thomas W. Ebbesen

ISIS, Laboratoire des Nanostructures,

Université de Strasbourg and CNRS,

8 allée Gaspard Monge, 67000 Strasbourg, France

(Dated: November 10, 2021)

Abstract

Light interacts differently with left and right handed three dimensional chiral objects, like helices, and this leads to the phenomenon known as optical activity. Here, by applying a polarization tomography, we show experimentally, for the first time in the visible domain, that chirality has a different optical manifestation for twisted planar nanostructured metallic objects acting as isolated chiral metaobjects. Our analysis demonstrate how surface plasmons, which are lossy bidimensional electromagnetic waves propagating on top of the structure, can delocalize light information in the just precise way for giving rise to this subtle effect.

I. INTRODUCTION

Since the historical work of Arago [1] and Pasteur [2], chirality (the handedness of nature) has generally been associated with optical activity, that is the rotation of the plane of polarisation of light passing through a medium lacking mirror symmetry [3, 4]. Optical activity is nowadays a very powerful probes of structural chirality in varieties of system. However, two-dimensional chiral structures, such as planar molecules, were not expected to display any chiral characteristics since simply turning the object around leads to the opposite handedness (we remind that a planar structure is chiral if it can not be brought into congruence with its mirror image unless it is lifted from the plane). This fundamental notion was recently challenged in a pioneering study where it was shown that chirality has a distinct signature from optical activity when electromagnetic waves interact with a 2D chiral structure and that the handedness can be recognized [5]. While the experimental demonstration was achieved in the giga-Hertz (mm) range for extended 2D structures, the question remained whether this could be achieved in the optical range since the laws of optics are not simply scalable when downsizing to the nanometer level. Here we report genuine optical planar chirality for a single subwavelength hole surrounded by left and right handed Archimedian spirals milled in a metallic film. Key to this finding is the involvement of surface plasmons, lossy electromagnetic waves at the metal surfaces, and the associated planar spatial dispersion [6, 7]. Our results reveal how, in a stringent and unusual way, this optical phenomenon connects concepts of chirality, reciprocity and broken time symmetry.

We remind that partly boosted by practical motivations, such as the quest of negative refractive lenses [8] or the possibility to obtain giant optical activity for applications in optoelectronics, there is currently a renewed interest [8–18] in the optical activity in artificial photonic media with planar chiral structures. It was shown for instance that planar gammadionic structures, which have by definition no axis of reflection but a four-fold rotational invariance [9, 11], can generate optical activity with giant gyrotropic factors [12, 16–18]. Importantly, and in contrast to the usual three dimensional (3D) chiral medium (like quartz and its helicoidal structure [3, 19]), planar chiral structures change their observed handedness when the direction of light is reversed through the system [9, 20]. This challenged Lorentz principle of reciprocity [4] (which is known to hold for any linear non magneto-optical media) and stirred up considerable debate [9, 10, 12, 21] which came to the conclusion that optical

activity cannot be a purely 2D effect and always requires a small dissymmetry between the two sides of the system [12, 16–18]. Nevertheless Zheludev and colleagues did demonstrate in the GHz spectrum that a pure 2D chiral structure lacking rotational symmetry can have an optical signature which is distinct from optical activity [5]. They went on to predict that it should be possible to observe the same phenomena in the optical range by scaling down their fish-scale structure and playing on localized plasmons [22]. Following a different strategy, we show here that SP waves propagating on a 2D metal chiral grating resonantly excited by light provide an elegant solution to generate planar optical chirality in the visible.

II. EXPERIMENTS AND RESULTS

This is a challenging issue as it leads to two fundamental points which are apparently incompatible. On the one hand, finding such a 2D chiral effect in the optical domain is not equivalent to a simple rescaling of the problem from the GHz to the visible part of the spectrum. Indeed, losses in metal become predominant at the nanometer scale so that the penetration length of light through any chiral structure will become comparable to the thickness of the structure. In-depth spatial dispersion along the propagation direction of light will hence be induced, corresponding to the usual 3D optical activity [11–18]. One thus expects optical activity, through the losses, to be a more favorable channel than 2D optical chirality. On the other hand, losses (i.e., broken time invariance at the macroscopic scale) are necessary to guarantee planar chiral behavior [5, 22]. With this in mind, we chose to make single SP structures such as a single hole in an optically thick metal film surrounded by an Archimedian spirals (Figure 1) which can provide all the necessary ingredients for observing 2D optical chirality. It is a 2D structure lacking point symmetry, that is rotational and mirror invariances. At the same time, it resonates due to coupling to surface plasmons which, as lossy waves, represent a natural way for delocalizing information along a planar interface, moving in-depth losses to the surface. Importantly, the thickness of the metal film optically decouples both interface [23], and consequently only the structured chiral side is involved in the 2D optical chiral effect reported here. Finally, the structures gives rise to enhanced transmission [7] enabling high optical throughput for all the characterization measurements.

Using focus ion beam (FIB), we milled in an opaque gold film a clockwise (right \mathcal{R}) or anticlockwise (left \mathcal{L}) Archimedian spiral grooves around a central subwavelength hole. The polar equation (ρ, θ) of the left handed Archimedian spiral is $\rho = P \cdot \theta / (2\pi)$, and the right handed enantiomeric spiral is obtained by reflection across the y axis (see Fig. 1). The

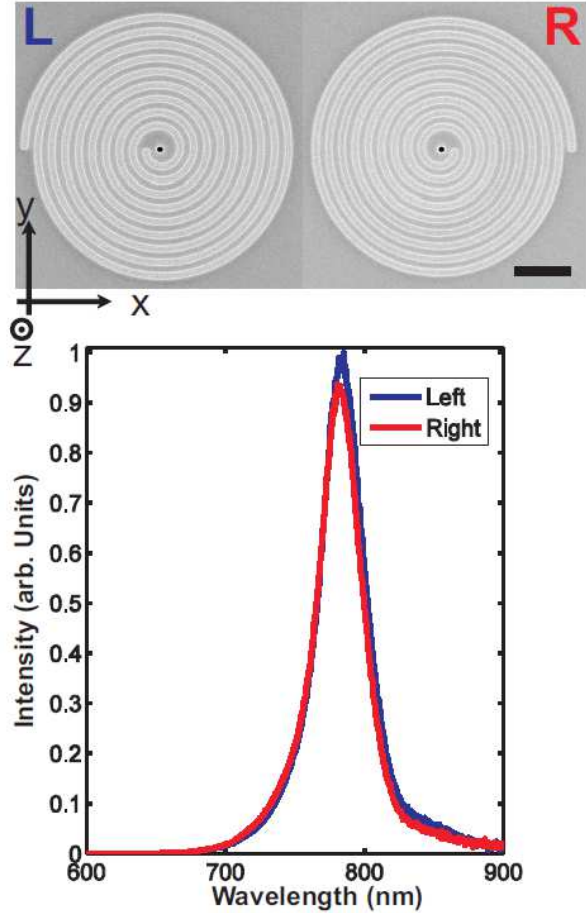


FIG. 1: Chiral plasmonic metamolecules. On the top panel: scanning electron micrographs of the left (L) and right (R) handed enantiomer (mirror image) planar chiral structures investigated. The scale bare is $3 \mu\text{m}$ long. The parameters characterizing the structure are the following: hole diameter $d = 350 \text{ nm}$, film thickness $h = 310 \text{ nm}$, grating period $P = 760 \text{ nm}$, groove width $w = 370 \text{ nm}$, and groove depth $s = 80 \text{ nm}$. The structures are milled, with a focus ion beam, in a gold film deposited on a glass substrate. On the bottom panel: transmission spectra at normal incidence of individual left (blue curve) and right handed (red curve) Archimede spirals illuminated from the air side.

geometrical parameter P is the radial grating period and we take its value equal to the

SP wavelength $\lambda_{SP} \simeq 760$ nm (for an excitation at $\lambda \simeq 780$ nm). We recorded optical transmission spectra at normal incidence with unpolarized light for both isolated structures (Fig. 1). As it can be seen, both enantiomers behave like resonant antennas with quasi identical transmission properties. This resonant behaviour is a direct indication of the SP excitation by the grating similarly to what is observed for circular antennas [24].

To observe and fully characterize the optical signature of planar chirality we perform a full polarization tomography [25, 26] with the aim of determining the 4×4 Mueller matrix \mathcal{M} associated with each enantiomer. Experimental results $\mathcal{M}_{\mathcal{L}}^{\text{exp.}}$, and $\mathcal{M}_{\mathcal{R}}^{\text{exp.}}$ respectively obtained for left and right handed spirals are given in appendixes A and B. Here the important point is that the degree of purity F of the Mueller matrices [25] is near unity with $F(\mathcal{M}_{\mathcal{L}}^{\text{exp.}}) \simeq 0.967$ and $F(\mathcal{M}_{\mathcal{R}}^{\text{exp.}}) \simeq 0.939$. This shows that the coherence in polarization is not degraded by the structure and that we can therefore restrict our discussion to Jones matrices [3, 25]. In the convenient left $|L\rangle$ and right $|R\rangle$ circular polarization basis, these Jones matrices tie the excitation $[E_L^{\text{in}}, E_R^{\text{in}}]$ to the transmitted $[E_L^{\text{out}}, E_R^{\text{out}}]$ electric fields. In the case of planar chiral structures displaying 2D chiral activity, they have the following form [5, 22]:

$$\mathcal{J}_{\mathcal{L}}^{\text{th.}} = \begin{pmatrix} A & B \\ C & A \end{pmatrix}, \mathcal{J}_{\mathcal{R}}^{\text{th.}} = \begin{pmatrix} A & C \\ B & A \end{pmatrix}, \quad (1)$$

where A , B and C are complex valued numbers such that $|B| \neq |C|$. This inequality account for chirality. Being non diagonal, these matrices correspond to polarization converter elements with no rotational invariance around the z axis (Fig. 1). They are thus fundamentally different from Jones matrices associated with optical activity, e.g., gamma-dions. Importantly the conditions $|B| \neq |C|$ implies the non unitarity of $\mathcal{J}_{\mathcal{L},\mathcal{R}}^{\text{th.}}$ which means that reversing the light path through the chiral structures is not equivalent to reversing the time. From equation (1) we deduce the associated theoretical forms for the Mueller matrices $\mathcal{M}_{\mathcal{L}}^{\text{th.}}$, $\mathcal{M}_{\mathcal{R}}^{\text{th.}}$ (see appendix C) which are used to fit $\mathcal{J}_{\mathcal{L}}$ and $\mathcal{J}_{\mathcal{R}}$ from experimental results. After normalization by A we deduce

$$\mathcal{J}_{\mathcal{L}}^{\text{fit}} = \begin{pmatrix} 1.000 & 0.166 + i0.221 \\ -0.131 + i0.099 & 1.000 \end{pmatrix},$$

$$\mathcal{J}_{\mathcal{R}}^{\text{fit}} = \begin{pmatrix} 1.000 & -0.129 + i0.098 \\ 0.170 + i0.230 & 1.000 \end{pmatrix}. \quad (2)$$

These matrices indeed satisfy the chirality criteria of equation (1) within the $\sim 1\%$ uncertainty evaluated from the degree of purity of the Mueller matrix of the empty setup.

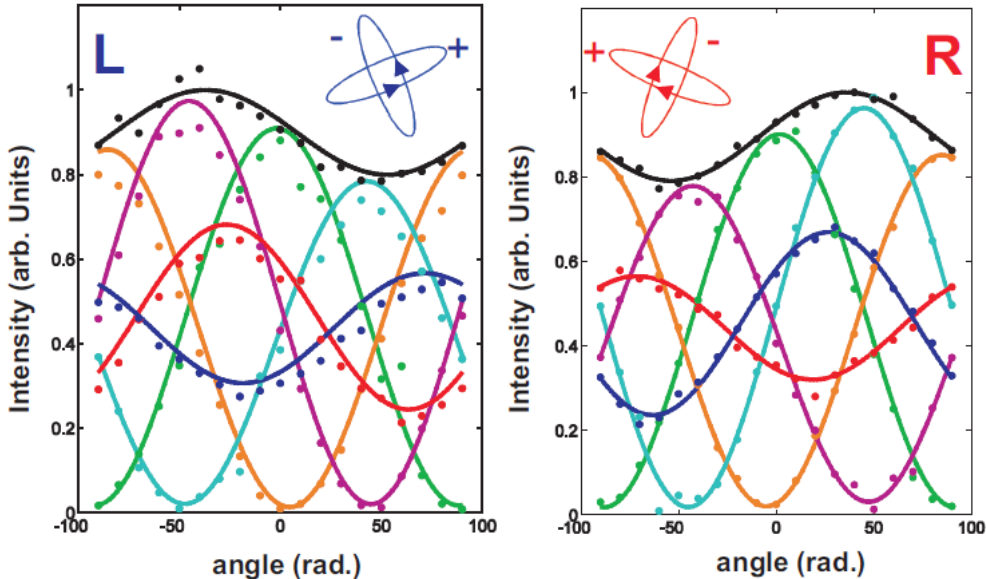


FIG. 2: Analysis of the polarization states for an input light with variable linear polarization for both the left (left panel) and right handed (right panel) individual chiral structures of Fig. 1. The data points (acquired with a laser light at $\lambda = 780$ nm) are compared to the predictions from equation (2) (continuous curves) for respectively the transmitted intensity analyzed along the direction: $|x\rangle$ (green), $|y\rangle$ (yellow), $|+45^\circ\rangle$ (cyan), $|-45^\circ\rangle$ (magenta), $|L\rangle$ (red), and $|R\rangle$ (blue). The total transmitted intensity is also shown (black). The symmetries between both panel expected from group theory (see appendix D) are observed experimentally. The insets show in each panel the ellipses of polarization and the handedness (arrow) associated with the two corotating eigenstates associated with the Jones matrix \mathcal{J}_L (blue) and \mathcal{J}_R (red).

III. DISCUSSION AND CONCLUSION

To illustrate the polarization conversion properties of our chiral structures, we compare in Fig. 2 theory and experiment when the input state is linearly polarized and when the output transmitted intensity is analyzed along different orthogonal directions. A good agreement between the measurements and the theoretical predictions deduced from the Jones matri-

ces (see appendix D) is clearly seen, together with the mirror symmetries between the two enantiomers. Importantly, these symmetries also imply that for unpolarized light, and in complete consistency with Fig. 1, the total intensity transmitted by the structures is independent of the chosen enantiomer. Furthermore, the conversion of polarization is well (geometrically) illustrated by using the Poincaré sphere representation [25]. Indeed, as shown in Fig. 3, the Mueller matrix defines a geometrical transformation which projects the unit Poincaré sphere, drawn by the input Stokes vector, on an output closed surface with typical radius $F(\mathcal{M}^{\text{exp.}}) \simeq 1$ in agreement with the absence of net depolarization as already noticed (from theory, $F(\mathcal{M}^{\text{th.}}) = 1$ exactly). Data shown on Fig. 2 are also plotted on this sphere. The input state draws a circle in the equator plane while the output state (for each enantiomer) draws a circle in a different plane, which center is not located at the center of the sphere. This is a direct manifestation of planar chirality (see appendix E). There is clearly an antisymmetrical behaviour between both enantiomers. The good agreement

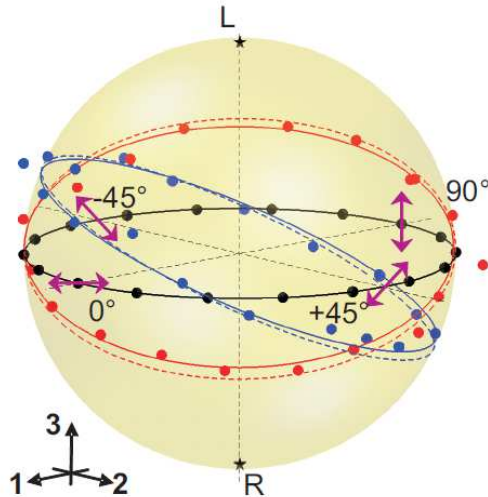


FIG. 3: Full polarization tomography. Poincaré sphere of unit radius associated with the input state represented by the Stokes vector \mathbf{X} [3, 25]. Also shown are the results of Fig. 2 for the left (blue) and right handed (red) structures if the linearly polarized incident state draw the black circle in the (X_1, X_2) equator plane of the input sphere. Data points are compared with the predictions from $\mathcal{M}_{\mathcal{L},\mathcal{R}}^{\text{exp.}}$ (continuous curves) and of equation (2) (dashed curves).

between the experiment and the prediction of equations (1,2) shows the sensitivity of the polarization tomography method and the high reliability of the FIB fabrication.

The degree of optical 2D chirality is quantified by diagonalizing $\mathcal{J}_{\mathcal{L}}^{\text{th.}}$ and $\mathcal{J}_{\mathcal{R}}^{\text{th.}}$. For $\mathcal{J}_{\mathcal{L}}^{\text{th.}}$, the eigenstates are $|\pm_{\mathcal{L}}\rangle = \sqrt{B}|L\rangle \pm \sqrt{C}|R\rangle$ associated with the eigenvalues $\lambda_{\mathcal{L}}(\pm) = A \pm \sqrt{(B \cdot C)}$. The eigenstates for $\mathcal{J}_{\mathcal{R}}^{\text{th.}}$ are obtained by permutation of B and C with consequently $\lambda_{\mathcal{L}}(\pm) = \lambda_{\mathcal{R}}(\pm)$. The scalar product $\langle +_{\mathcal{L}} | -_{\mathcal{L}} \rangle^{\text{th.}} = -\langle +_{\mathcal{R}} | -_{\mathcal{R}} \rangle^{\text{th.}} = (|B| - |C|)/(|B| + |C|)$ is the eigenstates Stokes parameter S_3/S_0 and provides a direct measurement of the degree of optical chirality. It also evaluates losses since the non-orthogonality of these two states is related to the necessary non-unitarity of the Jones matrix for planar chirality. We have $\langle +_{\mathcal{L}} | -_{\mathcal{L}} \rangle^{\text{fit}} \simeq 0.255$ and $\langle +_{\mathcal{R}} | -_{\mathcal{R}} \rangle^{\text{fit}} \simeq -0.277$, which, within experimental uncertainties, are in good agreement with the theoretical expectations. As shown in the insets of Fig. 2, both eigenstates of each structure (e.g., $|\pm_{\mathcal{L},\mathcal{R}}\rangle$) can be represented by two ellipses having the same axis ratio and the same handedness, but rotated 90° relative to each other. In agreement with the theoretical predictions, these polarization ellipses for $|\pm_{\mathcal{L}}\rangle$ and $|\pm_{\mathcal{R}}\rangle$ are mirror reflections. This behaviour is significantly different from the results obtained with optically active media [12–14, 16–18] where the eigenstates associated with a given enantiomer have opposite handedness [4]. This point, which reflects itself in the symmetry property of chiral Jones matrices, namely $\mathcal{J}_{\mathcal{L},\mathcal{R}}^{\text{th.}}(L, L) = \mathcal{J}_{\mathcal{L},\mathcal{R}}^{\text{th.}}(R, R) = A$, has far reaching consequences, as pointed out in reference [5]. It implies that a 2D plasmonic spiral mimics a Faraday medium when we reverse the light path and this even if the system, unlike a true Faraday medium, obeys rigorously to the principle of reciprocity [4, 5] (inversely, one can show that equation (1) results from both this requirement and the absence of mirror symmetry). It means that a photon coming from the second side will probe a structure of opposite chirality. After going through the structure and retracing back the light path with a mirror normal to the axis, the polarization state will be different at the end of journey from the initial one. This would be impossible for an optically active medium and is solely due to planar chirality. To summarize, our results therefore demonstrate that 2D chirality is possible in the visible domain in the absence of optical activity and add another element to the promising plasmonic toolkit.

IV. APPENDIX A: POLARIZATION TOMOGRAPHY SETUP.

We apply a procedure similar to the one considered in [26, 27] in order to record the Mueller matrix: a collimated laser beam at $\lambda = 785$ nm is focussed normally on the struc-

ture by using an objective L_1 ($\times 50$, numerical aperture=0.55). The transmitted light is collected and recollimated by using a second objective L_2 ($\times 40$, numerical aperture=0.6). The input and output states of polarization are respectively prepared and analyzed in the collimated part of the light path by using polarizers, half wave plates and quarter wave plates. A sketch of the setup is provided below (see Fig. 4).

The Mueller matrix is built by applying an experimental algorithm equivalent to the one

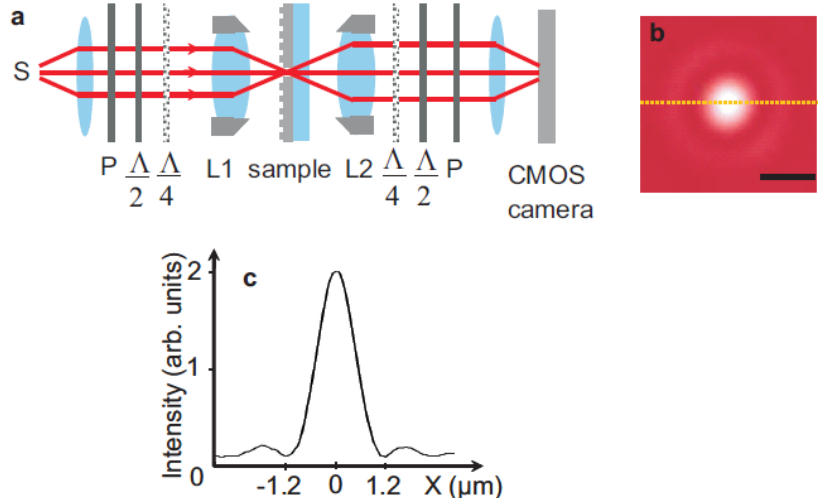


FIG. 4: Principle of the polarization experiment. (a), Sketch of the optical set up described in the text. The images are recorded by using a CMOS camera. (b), A typical image of the transmitting nanohole showing the Airy spot associated with diffraction by the optical microscope. The scale bar is 2 μm long. (c), Crosscut of the intensity profile along the yellow dotted line shown in (b).

described in [25]. More precisely, in order to write down the full Mueller matrix, we measured here 6×6 intensity projections corresponding to the 6 unit vectors $|x\rangle$, $|y\rangle$, $|+45^\circ\rangle$, $|-45^\circ\rangle$, $|L\rangle$, and $|R\rangle$ for the input and the output polarizations. Actually only 16 measures are needed to determine \mathcal{M} [25]. Our actual procedure is thus more than sufficient to obtain \mathcal{M} .

The isotropy of the setup was first checked by measuring the Mueller matrix $\mathcal{M}^{\text{glass}}$ with a glass substrate. Up to a normalization constant, we deduced that $\mathcal{M}^{\text{glass}}$ is practically identical to the identity matrix \mathcal{I} with individual elements deviating by no more than 0.02. More precisely, the optical depolarization (i. e, the losses in polarization coherence) can be precisely quantified through the degree of purity of the Mueller matrix defined by [25]

$F(\mathcal{M}) = \left(\frac{\text{Tr}[\mathcal{M}^\dagger \mathcal{M}] - \mathcal{M}_{00}^2}{3\mathcal{M}_{00}^2} \right)^{1/2} \leq 1$. Here we measured $F(\mathcal{M}^{\text{glass}}) = 0.9851$. It implies that the light is not depolarized when going through the setup and that consequently we can rely on our measurement procedure for obtaining \mathcal{M} .

Two important points must be noted here: On the one hand we varied the incident illumination spot size on the sample between 2 and 20 μm without affecting the matrix, i. e., without introducing additional depolarisation. In the rest of the experiment on chiral structures we consider the case of a large gaussian spot with FWHM=20 μm in order to illuminate the whole individual spiral. On the other hand, it can be observed that in our experiments the polarization in the Airy spot (see Fig. 4b) is homogeneous. This implies that we are actually doing the polarization tomography of the central transmitting hole, i. e., we are dealing only with the SU(2) point symmetry of the Mueller Matrix. This situation clearly contrasts with previous SOP tomography measurements on metallic hole arrays in which the polarization degrees of freedom were mixed with spatial information responsible for SPP-induced depolarization [26].

V. APPENDIX B: EXPERIMENTAL MUELLER MATRICES.

The experimental Mueller matrices deduced from the polarization tomography are after normalization of $\mathcal{M}_{00}^{\text{exp.}}$:

$$\begin{aligned} \mathcal{M}_{\mathcal{L}}^{\text{exp.}} &= \begin{pmatrix} 1.000 & 0.031 & -0.107 & -0.029 \\ 0.029 & 0.958 & 0.044 & -0.251 \\ -0.105 & 0.037 & 0.953 & 0.287 \\ 0.029 & 0.261 & -0.282 & 0.809 \end{pmatrix}, \\ \mathcal{M}_{\mathcal{R}}^{\text{exp.}} &= \begin{pmatrix} 1.000 & 0.035 & 0.111 & 0.023 \\ 0.027 & 0.949 & -0.051 & 0.246 \\ 0.096 & -0.034 & 0.943 & 0.267 \\ -0.011 & -0.252 & -0.277 & 0.745 \end{pmatrix}. \end{aligned} \quad (3)$$

We have $F(\mathcal{M}_{\mathcal{L}}^{\text{exp.}}) \simeq 0.967$ and $F(\mathcal{M}_{\mathcal{R}}^{\text{exp.}}) \simeq 0.939$.

We must also note that the normalization used here neglects a small additional coefficient of proportionality $|\mathcal{M}_{\mathcal{L}ij}^{\text{exp.}}/\mathcal{M}_{\mathcal{R}ij}^{\text{exp.}}| \simeq 0.954$ imputed to experimental errors and uncertainties.

We also recorded the Mueller matrix of the set up with the glass substrate only. Up to a normalization factor we deduced

$$\mathcal{M}^{\text{glass}} = \begin{pmatrix} \underline{1.0000} & 0.0060 & -0.0040 & -0.0070 \\ -0.0030 & \underline{0.9851} & -0.0010 & 0.0020 \\ -0.0020 & 0.0020 & \underline{0.9965} & 0.0030 \\ -0.0050 & -0.0040 & 0.0030 & \underline{0.9821} \end{pmatrix} \quad (4)$$

which satisfies $\mathcal{M}^{\text{glass}} \simeq \mathcal{I}$ with \mathcal{I} the identity matrix. It implies that the optical set up do not induce depolarization and that consequently we can rely on our measurement procedure for obtaining \mathcal{M} .

VI. APPENDIX C: THEORETICAL MUELLER MATRICES.

The precise form of the theoretical Mueller matrix $\mathcal{M}_{\mathcal{L}}^{\text{th.}}$ deduced from equation (1) is

$$\mathcal{M}_{\mathcal{L}}^{\text{th.}} = \begin{pmatrix} \mathcal{M}_{00}^{\text{th.}} & \mathcal{M}_{01}^{\text{th.}} & \mathcal{M}_{02}^{\text{th.}} & \mathcal{M}_{03}^{\text{th.}} \\ \mathcal{M}_{01}^{\text{th.}} & \mathcal{M}_{11}^{\text{th.}} & \mathcal{M}_{12}^{\text{th.}} & \mathcal{M}_{13}^{\text{th.}} \\ \mathcal{M}_{02}^{\text{th.}} & \mathcal{M}_{12}^{\text{th.}} & \mathcal{M}_{22}^{\text{th.}} & \mathcal{M}_{23}^{\text{th.}} \\ -\mathcal{M}_{03}^{\text{th.}} & -\mathcal{M}_{13}^{\text{th.}} & -\mathcal{M}_{23}^{\text{th.}} & \mathcal{M}_{33}^{\text{th.}} \end{pmatrix}. \quad (5)$$

with $\mathcal{M}_{00}^{\text{th.}} = (2|A|^2 + |B|^2 + |C|^2)/2$, $\mathcal{M}_{01}^{\text{th.}} = \text{Re}[BA^* + AC^*]$, $\mathcal{M}_{02}^{\text{th.}} = \text{Im}[AB^* + CA^*]$, $\mathcal{M}_{03}^{\text{th.}} = (|C|^2 - |B|^2)/2$, $\mathcal{M}_{11}^{\text{th.}} = |A|^2 + \text{Re}[B^*C]$, $\mathcal{M}_{12}^{\text{th.}} = \text{Im}[B^*C]$, $\mathcal{M}_{13}^{\text{th.}} = \text{Re}[AC^* - BA^*]$, $\mathcal{M}_{22}^{\text{th.}} = |A|^2 - \text{Re}[B^*C]$, $\mathcal{M}_{23}^{\text{th.}} = \text{Re}[CA^* - AB^*]$, $\mathcal{M}_{33}^{\text{th.}} = (2|A|^2 - |B|^2 - |C|^2)/2$. Similar formula are obtained for $\mathcal{M}_{\mathcal{R}}^{\text{th.}}$ after permuting B and C .

From the previous relations we deduce the useful equations (valid for $\mathcal{M}_{\mathcal{L}}^{\text{th.}}$)

$$\begin{aligned} B/A &= \frac{\mathcal{M}_{01}^{\text{th.}} - \mathcal{M}_{13}^{\text{th.}}}{\mathcal{M}_{00}^{\text{th.}} + \mathcal{M}_{33}^{\text{th.}}} + i \frac{\mathcal{M}_{23}^{\text{th.}} - \mathcal{M}_{02}^{\text{th.}}}{\mathcal{M}_{00}^{\text{th.}} + \mathcal{M}_{33}^{\text{th.}}} \\ C/A &= \frac{\mathcal{M}_{01}^{\text{th.}} + \mathcal{M}_{13}^{\text{th.}}}{\mathcal{M}_{00}^{\text{th.}} + \mathcal{M}_{33}^{\text{th.}}} + i \frac{\mathcal{M}_{23}^{\text{th.}} + \mathcal{M}_{02}^{\text{th.}}}{\mathcal{M}_{00}^{\text{th.}} + \mathcal{M}_{33}^{\text{th.}}} \end{aligned} \quad (6)$$

Together with equation (3) equation (6) allow us to fit B/A and C/A if we replace $\mathcal{M}^{\text{th.}}$ by $\mathcal{M}_{\mathcal{L}}^{\text{exp.}}$ (a similar procedure is applicable to $\mathcal{M}_{\mathcal{R}}^{\text{exp.}}$ after permuting B and C).

The best fit we obtained (see equation (2)) are:

$$\begin{aligned} \mathcal{M}_{\mathcal{L}}^{\text{fit}} &= \begin{pmatrix} 1.000 & 0.033 & -0.116 & -0.023 \\ 0.033 & 0.951 & 0.043 & -0.282 \\ -0.116 & 0.043 & 0.951 & 0.304 \\ 0.023 & 0.282 & -0.304 & 0.902 \end{pmatrix}, \\ \mathcal{M}_{\mathcal{R}}^{\text{fit}} &= \begin{pmatrix} 1.000 & 0.0359 & 0.125 & 0.026 \\ 0.039 & 0.949 & -0.044 & 0.283 \\ 0.125 & -0.044 & 0.948 & 0.311 \\ -0.026 & -0.283 & -0.311 & 0.897 \end{pmatrix}. \end{aligned} \quad (7)$$

From theory we can deduce that $F(\mathcal{M}_{\mathcal{L},\mathcal{R}}^{\text{th.}}) = 1$ (i.e., after normalization by $\mathcal{M}_{00}^{\text{th.}}$). We have thus $F(\mathcal{M}_{\mathcal{L},\mathcal{R}}^{\text{fit}}) = 1$

VII. APPENDIX D: SYMMETRIES DUE TO CHIRALITY [INTERPRETING FIGURE 2].

Let $|\Psi_{\text{in}}\rangle = E_x|x\rangle + E_y|y\rangle$ and $|\Psi_{\text{out}}\rangle = E'_x|x\rangle + E'_y|y\rangle$ be respectively the incident and transmitted electric fields when we consider the left handed planar chiral structure. We have

$$|\Psi_{\text{out}}\rangle = \hat{\mathcal{J}}_{\mathcal{L}}|\Psi_{\text{in}}\rangle \quad (8)$$

where $\hat{\mathcal{J}}_{\mathcal{L}}$ is the operator associated with the Jones matrix $\mathcal{J}_{\mathcal{L}}$. The mathematical definition of planar chirality is that whatever the mirror symmetry operation $\hat{\Pi}$ in the plane X-Y we have $\hat{\mathcal{J}}\hat{\Pi} - \hat{\Pi}\hat{\mathcal{J}} \neq 0$. It equivalently states that $\hat{\Pi}\hat{\mathcal{J}}\hat{\Pi}^{-1} \neq \hat{\mathcal{J}}$. If we consider for example the mirror reflection through the Y axis (see Fig. 1) we have the matrix representation (in the cartesian basis) $\Pi = \Pi^{-1} = \begin{pmatrix} -1 & 0 \\ 0 & 1 \end{pmatrix}$ and consequently

$$\hat{\Pi}\hat{\mathcal{J}}_{\mathcal{L}}\hat{\Pi}^{-1} = \hat{\mathcal{J}}_{\mathcal{R}} \neq \hat{\mathcal{J}}_{\mathcal{L}} \quad (9)$$

which agrees with equation (1) and constitutes an other optical definition of chirality.

The previous equations are used in order to interpret the results of Fig. 3 of the main article.

Indeed from equations (8) and (9) we obtain

$$\hat{\Pi}|\Psi_{\text{out}}\rangle = \hat{\mathcal{J}}_{\mathcal{R}}\hat{\Pi}|\Psi_{\text{in}}\rangle. \quad (10)$$

The input state considered in Fig. 2 is a linearly polarized light $|\theta\rangle = \sin(\theta)|x\rangle + \cos(\theta)|y\rangle$ (the angle is measured relatively to the Y axis) and the transmitted intensity projected along a direction of analysis $|i\rangle$ (i.e, $|x\rangle$, $|y\rangle$, $|+45^\circ\rangle$, $|-45^\circ\rangle$, $|L\rangle$, and $|R\rangle$) is written $I_i^{(\text{Left})}(\theta) = |\langle i|\Psi_{\text{out}}\rangle|^2 = |\langle i|\hat{\mathcal{J}}_{\mathcal{L}}|\theta\rangle|^2$. Similarly we also write $I_i^{(\text{Right})}(\theta) = |\langle i|\hat{\mathcal{J}}_{\mathcal{R}}|\theta\rangle|^2$. From equation (10) we deduce:

$$\langle i'|\hat{\mathcal{J}}_{\mathcal{L}}|\theta\rangle = \langle i|\hat{\mathcal{J}}_{\mathcal{L}}|-\theta\rangle, \quad (11)$$

where we used $|i'\rangle = \hat{\Pi}^{-1}|i\rangle = \hat{\Pi}|i\rangle$ and $|-\theta\rangle = \hat{\Pi}|\theta\rangle$. We consequently have:

$$\begin{aligned} I_{\text{total}}^{(\text{Left})}(\theta) &= I_{\text{total}}^{(\text{Right})}(-\theta), \\ I_{x,y}^{(\text{Left})}(\theta) &= I_{x,y}^{(\text{Right})}(-\theta), \\ I_{\pm 45^\circ}^{(\text{Left})}(\theta) &= I_{\mp 45^\circ}^{(\text{Right})}(-\theta), \\ I_{L,R}^{(\text{Left})}(\theta) &= I_{R,L}^{(\text{Right})}(-\theta). \end{aligned} \quad (12)$$

Such symmetries are clearly visible in Fig. 2 and correspond to a direct signature of optical chirality in the planar systems considered.

VIII. APPENDIX E: PLANAR CHIRALITY ON THE POINCARÉ SPHERE [INTERPRETING FIGURE 3]

We remind that the Stokes parameters associated with a polarization state of light $|\Psi\rangle$ are defined by

$$\begin{aligned} S_0 &= I_x + I_y, \quad S_1 = I_x - I_y \\ S_2 &= I_{+45^\circ} - I_{-45^\circ}, \quad S_3 = I_L - I_R, \end{aligned} \quad (13)$$

where I_i are projection measurement along the direction i , i.e, $I_i = |\langle i|\Psi\rangle|^2$. The Stokes vector \mathbf{X} is a convenient representation of such a state. We have $\mathbf{X} = X_1\mathbf{x}_1 + X_2\mathbf{x}_2 + X_3\mathbf{x}_3$ with $X_1 = S_1/S_0$, $X_2 = S_2/S_0$, $X_3 = S_3/S_0$ and with $(\mathbf{x}_1, \mathbf{x}_2, \mathbf{x}_3)$ a cartesian orthogonal and normalized vector basis.

The coherent input state satisfies the normalization [25] $|\mathbf{X}| = 1$, that is the vector draw a Poincaré sphere of unit radius in the space X_1, X_2, X_3 . The transmitted output state after

interaction with the left or right handed structure is defined by the relation

$$\begin{pmatrix} S_{\mathcal{L},\mathcal{R};0} \\ S_{\mathcal{L},\mathcal{R};1} \\ S_{\mathcal{L},\mathcal{R};2} \\ S_{\mathcal{L},\mathcal{R};3} \end{pmatrix} = \mathcal{M}_{\mathcal{L},\mathcal{R}} \begin{pmatrix} S_0 \\ S_1 \\ S_2 \\ S_3 \end{pmatrix}. \quad (14)$$

The output state defines a Stokes vector $\mathbf{X}_{\mathcal{L},\mathcal{R}}$ such that $|\mathbf{X}_{\mathcal{L},\mathcal{R}}| \leq 1$. A typical value for this radius is given by $F(\mathcal{M}_{\mathcal{L},\mathcal{R}})$.

If the input state is linearly polarized the input Stokes vector is:

$$\mathbf{X}^{\text{in}}(\theta) = \begin{pmatrix} \cos(2\theta) \\ \sin(2\theta) \\ 0 \end{pmatrix}, \quad (15)$$

and draw a circle (Σ_{in}) along the equator contained in the plane X_1, X_2 of the unit radius Poincaré sphere. Using equation (14) the output Stokes vector is now a function of θ : $\mathbf{X}_{\mathcal{L},\mathcal{R}}(\theta)$ drawing a closed curve ($\Sigma_{\mathcal{L},\mathcal{R}}$) (see Fig. 3) which is the image, through the Mueller matrix transformation, of the equator circle (Σ_{in}) above mentioned. Importantly, since the Mueller matrix \mathcal{M} given by equation (5) represents a linear relation connecting \mathbf{X}^{in} to \mathbf{X}^{out} , we conclude that the image of the incident polarization state contained in the equator plane X_1, X_2 through \mathcal{M} must also be contained in a plane in the space X_1, X_2, X_3 .

To analyze this point more in details we consider the normalized Vector product

$$\mathbf{n}_{\mathcal{L},\mathcal{R}} = \frac{(\mathbf{X}_{\mathcal{L},\mathcal{R}}(0) - \mathbf{X}_{\mathcal{L},\mathcal{R}}(2\pi/3)) \times (\mathbf{X}_{\mathcal{L},\mathcal{R}}(0) - \mathbf{X}_{\mathcal{L},\mathcal{R}}(\pi/2))}{|(\mathbf{X}_{\mathcal{L},\mathcal{R}}(0) - \mathbf{X}_{\mathcal{L},\mathcal{R}}(2\pi/3)) \times (\mathbf{X}_{\mathcal{L},\mathcal{R}}(0) - \mathbf{X}_{\mathcal{L},\mathcal{R}}(\pi/2))|} \quad (16)$$

and we write it

$$\mathbf{n}_{\mathcal{L},\mathcal{R}} = \begin{pmatrix} U_{\mathcal{L},\mathcal{R}} \\ V_{\mathcal{L},\mathcal{R}} \\ W_{\mathcal{L},\mathcal{R}} \end{pmatrix}, \quad (17)$$

with $|U_{\mathcal{L},\mathcal{R}}|^2 + |V_{\mathcal{L},\mathcal{R}}|^2 + |W_{\mathcal{L},\mathcal{R}}|^2 = 1$. It represents a typical normal to the closed curve ($\Sigma_{\mathcal{L},\mathcal{R}}$). We have

$$\mathbf{n}_{\mathcal{L}} = \begin{pmatrix} 0.2845 \\ -0.3065 \\ -0.9084 \end{pmatrix}, \mathbf{n}_{\mathcal{R}} = \begin{pmatrix} 0.2861 \\ 0.3139 \\ 0.95053 \end{pmatrix}. \quad (18)$$

Actually, if each curve $(\Sigma_{\mathcal{L},\mathcal{R}})$ is contained in a (different) plane $P_{\mathcal{L},\mathcal{R}}$ we must have

$$\mathbf{n}_{\mathcal{L},\mathcal{R}} \cdot (\mathbf{X}_{\mathcal{L},\mathcal{R}}(\theta) - \mathbf{X}_{\mathcal{L},\mathcal{R}}(0)) = 0 \quad (19)$$

for every θ . This was indeed checked numerically up to a precision of 10^{-11} . It was also checked that $|\mathbf{X}_{\mathcal{L},\mathcal{R}}(\theta)| = 1$ up to the same precision. This proves that each curve $(\Sigma_{\mathcal{L},\mathcal{R}})$ must be a circle. The equations of the two planes $P_{\mathcal{L},\mathcal{R}}$ are given by $\mathbf{n}_{\mathcal{L},\mathcal{R}} \cdot (\mathbf{X} - \mathbf{X}_{\mathcal{L},\mathcal{R}}(0)) = 0$ where \mathbf{X} is the Stokes vector associated with a running point belonging to each plane. We write

$$U_{\mathcal{L},\mathcal{R}}X_1 + V_{\mathcal{L},\mathcal{R}}X_2 + W_{\mathcal{L},\mathcal{R}}X_3 + D_{\mathcal{L},\mathcal{R}} = 0 \quad (20)$$

with $D_{\mathcal{L}} = -0.0237$ and $D_{\mathcal{R}} = -0.0266$. $|D_{\mathcal{L},\mathcal{R}}|$ represents the distance separating the center of the circle $(\Sigma_{\mathcal{L},\mathcal{R}})$ to the origin of the Poincaré sphere. This proves that the planes are not going through the center of the sphere. It was checked after lengthy calculations that if $|B| = |C|$ in the Jones matrix (see equation (1)) then $D = 0$. This shows that the property $|D_{\mathcal{L},\mathcal{R}}| \neq 0$ is a characteristic of planar chirality (i.e, the condition $|B| \neq |C|$). The radius of each circle $(\Sigma_{\mathcal{L},\mathcal{R}})$ is given by $r_{\mathcal{L},\mathcal{R}} = \sqrt{(1 - D_{\mathcal{L},\mathcal{R}}^2)}$ and we have $r_{\mathcal{L}} = 0.9997$ and $r_{\mathcal{R}} = 0.9996$ which are slightly smaller than $r = 1$ in agreement with the fact that $P_{\mathcal{L},\mathcal{R}}$ are not going through the center of the sphere.

-
- [1] D. -F. M. Arago, "Mémoire sur une modification remarquable qu'éprouvent les rayons lumineux dans leur passage à travers certains corps diaphanes, et sur quelques autres nouveaux phénomènes d'optique," *Mém. Inst. France, Part I* **12** (1811).
 - [2] L. Pasteur, "Mémoire sur la relation qui peut exister entre la forme cristalline et la composition chimique, et sur la cause de la polarization rotatoire," *C. R. Acad. Sci. Paris* **26**, 535-539 (1848).
 - [3] E. Hecht, *Optics 2nd ed.* (Addison-Wesley, Massachusetts, 1987).
 - [4] L. D. Landau, E. M. Lifshitz, L. P. Pitaevskii, *Electrodynamics of continuous media 2nd ed.* (Pergamon, New York, 1984).
 - [5] V. A. Fedotov, P. L. Mladyonov, S. L. Prosvirnin, A. V. Rogacheva, Y. Chen and N. I. Zheludev, "Asymmetric propagation of electromagnetic waves through a planar chiral structure," *Phys. Rev. Lett.* **97**, 167401 (2006).

- [6] W. L. Barnes, A. Dereux, T. W. Ebbesen, "Surface plasmon subwavelength optics," *Nature* **424**, 824 (2003).
- [7] C. Genet, T. W. Ebbesen, "Light in tiny holes," *Nature* **445**, 39-46 (2007).
- [8] J. B. Pendry, "A chiral route to negative refraction," *Science* **306**, 1353-1355 (2004).
- [9] A. Papakostas, A. Potts, D. M. Bagnall, S. L. Prosvirnin, H. J. Coles and N. I. Zheludev, "Optical manifestation of planar chirality," *Phys. Rev. Lett.* **90**, 107404 (2003).
- [10] A. S. Schwanecke, A. Krasavin, D. M. Bagnall, A. Potts, A. V. Zayats and N. I. Zheludev, "Broken time symmetry of light interaction with planar chiral nanostructures," *Phys. Rev. Lett.* **91**, 247404 (2003).
- [11] T. Vallius, K. Jefimovs, J. Turunen, P. Vahimaa and Y. Svirko, "Optical activity in subwavelength-period arrays of chiral metallic particles," *Appl. Phys. Lett.* **83**, 234-236 (2003).
- [12] M. Kuwata-Gonokami, N. Saito, Y. Ino, M. Kauranen, K. Jefimovs, T. Vallius, J. Turunen and Y. Svirko, "Giant optical activity in quasi-two-dimensional planar nanostructures," *Phys. Rev. Lett.* **95**, 227401 (2005).
- [13] B. K. Canfield, S. Kujala, K. Jefimovs, J. Turunen and M. Kauranen, "Linear and non-linear optical responses influenced by broken symmetry in an array of gold nanoparticles," *Opt. Express* **12**, 5418-5423 (2004).
- [14] B. K. Canfield, S. Kujala, K. Laiho, K. Jefimovs, J. Turunen and M. Kauranen, "Remarkable polarization sensitivity of gold nanoparticle arrays," *Opt. Express* **12**, 5418-5423 (2004).
- [15] W. Zhang, A. Potts, A. Papakostas and D. M. Bagnall, "Intensity modulation and polarization rotation of visible light by dielectric planar chiral materials," *Appl. Phys. Lett.* **86**, 231905 (2005).
- [16] M. Decker, M. W. Klein, M. Wegener and S. Linden, "Circular dichroism of planar chiral magnetic metamaterials," *Opt. Lett.* **32**, 856-858 (2007).
- [17] E. Plum, V. A. Fedotov, A. S. Schwanecke, N. I. Zheludev and Y. Chen "Giant optical gyrotropy due to electromagnetic coupling," *Appl. Phys. Lett.* **90**, 223113 (2007).
- [18] A. V. Rogacheva, V. A. Fedotov, A. S. Schwanecke and N. I. Zheludev, "Giant gyrotropy due to electromagnetic-field coupling in a bilayered chiral structure." *Phys. Rev. Lett.* **97**, 177401 (2006).
- [19] J. C. Bose, "On the rotation of plane of polarization of electric waves by a twisted structure." *Proc. R. Soc. London A* **63**, 146-152 (1898).

- [20] L. Hecht, L. D. Barron, “Rayleigh and Raman optical activity from chiral surfaces,” *Chem. Phys. Lett.* **225**, 525-530 (1994).
- [21] L. D. Barron, “Parity and optical activity,” *Nature* **238**, 17-19 (1972).
- [22] V. A. Fedotov, A. S. Schwanecke, N. I. Zheludev, V. V. Khardikov and S. L. Prosvirnin, “Asymmetric transmission of light and enantiomerically sensitive plasmon resonance in planar chiral nanostructures,” *Nano Lett.* **7**, 1996-1999 (2007).
- [23] A. Degiron and T. W. Ebbesen, “Analysis of the transmission process through a single aperture surrounded by periodic corrugations,” *Opt. Express* **12**, 3694-3700 (2004).
- [24] H. J. Lezec, A. Degiron, E. Devaux, R. A. Linke, L. Martin-Moreno, F. J. Garcia-Vidal and T. W. Ebbesen, “beaming light from a subwavelength aperture,” *Science* **297**, 820-822 (2002).
- [25] F. Le Roy-Brehonnet, B. Le Jeune, “Utilization of Mueller matrix formalism to obtain optical targets depolarization and polarization properties,” *Prog. Quant. Electr.* **21**, 109-151 (1997).
- [26] E. Altewisher, C. Genet, M. P. van Exter, J. P. Woerdman, P. F. A. Alkemade, A. van Zuuk and E. W. J. M. van der drift, “Polarization tomography of metallic nanohole arrays.” *Opt. Lett.* **30**, 90-92 (2005).
- [27] C. Genet, E. Altewischer, M. P. van Exter and J. P. Woerdman, “Optical depolarization induced by arrays of subwavelength metal holes,” *Phys. Rev. B.* **71**, 033409 (2005).